VISCOPLASTIC BEHAVIOR OF STEELS DURING WELDING

Yannick Vincent [1], Tobias Loose [2]

[1] ESI GROUP, 99 rue des Solets – PARC D'AFFAIRES SILIC 94150 RUNGIS

[2] Ingenieurbüro Tobias Loose GbR, Haid-und-Neu-Straße 7, 76131 Karlsruhe

Abstract

In most numerical simulations of welding, viscoplastic phenomena are neglected, because of shortness of the process. The aim of this paper is to accurately assess the effect of such phenomena upon predicted residual stresses and distortions, through comparison of simulations using both elastic-plastic and elastic-viscoplastic constitutive laws, and experiments. These experiments are performed on a mockup developed at INSA Lyon and especially designed for the study of the material behavior in the heat affected zone of a welded component; this mockup is sufficiently simple to allow for cheap 2D axisymmetric simulations, but nevertheless complex enough to represent a real welded structure, albeit in a schematic way. It is found that incorporation of viscous effects into the description of the material behavior has a marginal influence upon predicted residual stresses but a significant one upon predicted residual distortions, which agree much better with measured ones when viscous effects are accounted for.

Keywords: *Welding, viscoplasticity, experimental mockup, numerical simulation, SYSWELD®.*

1. Introduction

Welding of steel structures involves complex interactions between thermal, metallurgical and mechanical phenomena leading to residual stresses and distortions, which play a major role during subsequent service of these structures. Control of welding residual stresses, in particular, is of major interest in the nuclear industry. However, residual distortions are also of interest, in particular in the automotive industry. Such considerations have motivated important research programs in France on numerical simulations of welding, bringing together industrial partners (FRAMATOME ANP, Electricité de France, ESI GROUP) and the nuclear safety administration (Direction de la Sûreté des Installations Nucléaires). The essential aim of these programs is to improve the assessment of safety margins in simplified, conservative analyses of the welding processes involved in the manufacturing of nuclear components. It is clear, however, that their results can be useful for other industries. The work described here was performed within the context of these programs.

The reason why viscoplastic effects are disregarded in most welding simulations is that the duration of welding processes is quite short, so that it is generally thought to be insufficient for significant creep to occur.

The aim of this paper is precisely to accurately assess the influence of such a simplification upon predicted residual stresses and distortions. This cannot be inferred from previous results available in the literature, because even when viscous effects were incorporated in some simulation, no comparison was made with some “reference” simulation disregarding them. Such a comparison between simulations using elastic-plastic and elastic-viscoplastic

constitutive laws will be performed here; “reference” experimental results will also be presented and compared to those of the simulations.

In Section 2, we describe an experimental mockup developed at INSA Lyon and especially dedicated to the analysis of metallurgical and mechanical phenomena during welding. The geometry and the loading are chosen so as to maximize the influence of the material behavior in the heat affected zone (HAZ) (where viscous effects can take place) upon the overall response. The axisymmetric geometry is simple enough to allow for cheap simulations while remaining sufficiently complex to schematically represent an actual welded component. Quantities measured include temperature, proportions of metallurgical phases, displacements, and residual stresses and strains.

Numerical simulations with the SYSWELD Software incorporating viscous effects are then presented in Section 3. Incorporation of such effects is found to have a minor influence on predicted stresses, but a significant one on residual distortions, which are much better predicted, as compared to experiments, when viscous effects are accounted for.

2. Experimental mockup

2.1 Brief sketch

Since our aim is not to simulate some specific welding process, but to assess the influence of viscous effects in general during welding, it is preferable not to consider an actual welded structure, but a model geometry subjected to some simple, carefully controlled thermal loading. This will allow not only to simplify the numerical simulations but also, by avoiding fusion of the material, to eliminate poorly known phenomena such as convection in the molten pool, which are inevitably present in actual welding processes but would hamper here “neat”

comparison of experimental and numerical results and clear assessment of the influence of viscous effects.

An experimental mockup was thus developed at INSA Lyon in order to simulate a real welding operation in a simple, but not over-simplified way (which means that this mockup must not be a homogeneous specimen but a real, albeit simple structure). The geometry adopted is a circular disk, so as to allow for simple finite element simulations with an axisymmetric option, with a modest radius, so as to maximize the influence of the metallurgical and mechanical phenomena occurring in the HAZ upon the overall response. The heat input is controlled during all imposed thermal cycles in such a way that fusion does not occur. The material employed is the low alloy C-Mn steel used in French nuclear pressure vessels (16MND5 in the French AFNOR norm; see chemical composition in Tab. 1).

2.2 Experimental details

The original experimental procedure developed, named "INZAT Program", is schematically depicted in Fig. 1. The disk, with radius 160 mm and thickness 5 mm, lies on 3 radial alumina bars oriented at 0°, 120° and 240°. Illumination by a CO_2 laser provides an axisymmetric heat source around the center of the upper face. The heat input is chosen in such a way that the central part of the disk reaches an austenitic state during heating without melting : the maximum temperatures reached at the center of the upper and lower faces are 955 and 915°C respectively. Also, the thickness of the disk has been chosen sufficiently small for the through-the-thickness temperature gradient to be moderate, so as to generate essentially planar (radial and tangential) residual stresses, but not too small in order for the axial (out-of-plane) displacement to be nevertheless observable.

Two types of measurements are performed continuously during the whole experiment. Temperatures are recorded using 40 thermocouples welded along a diameter on the lower face. These measurements allow for the determination, using an inverse method, of the *a priori* unknown thermal boundary conditions, which are needed for the numerical simulations; these conditions include the heat input distribution and the radiative and convective heat transfer coefficients governing losses. Also, measurements of axial displacements are performed using 10 inductive sensors located at different points on the lower face of the disk.

After complete cooling of the disk, 4 types of measurements are made. First, residual stresses measurements are performed using X-ray diffraction. Second, the final deformed shape of the disk is recorded through measurement of the axial displacement along a diameter on both faces of the disk. Third, strain measurements are also carried out on the upper face using the numerical image correlation method[12]; these measurements are performed on the whole face in order to check for axisymmetry. Finally, a micrographic analysis coupled with micro- and macro-hardness measurements is performed in order to determine the metallurgical structure of an entire section of the disk.

The experimental error on measured stresses is not known accurately, but is thought to be at least of the order of 50 MPa at room temperature.

3. Comparison of experiments and elastic-plastic and elastic-viscoplastic analyses

3.1 Thermal, metallurgical and mechanical models used in the simulations

3.1.1 Generalities

Thermal properties are phase dependent, and metallurgical transformations involve latent heats; conversely, transformations of course depend on temperature. Thus the thermal and metallurgical calculations with SYSWELD are fully coupled and performed simultaneously, although they are presented separately here for clarity. On the other hand, heating arising from (visco)plastic dissipation, and influence of stresses and plastic strain on transformation kinetics are disregarded. Thus the thermo-metallurgical calculation is independent of the mechanical one, so they can be performed one after another, the results of the first being used in the second as input data.

3.1.2 Heat transfer

The heat conduction equation is solved using an enthalpic formulation[1] especially fit for optimal numerical treatment of latent heat effects. The data required are the specific heats of individual phases and the various transformation latent heats. These quantities are deduced, as functions of temperature (including the transition of the specific heat at the Curie temperature), from some measurement of the "overall" specific heat (which incorporates all phenomena in a global way) of a small specimen performed at a heating rate of 20°C/s, close to the actual one in the disk. The results of this measurement are displayed in the left part of Fig. 2.

It must be emphasized that the measurement of the "overall" specific heat is *not* used as a direct input for some classical thermal calculation, but, once again, to determine the specific heats of individual phases and transformation latent heats required for an *enthalpic* formulation coupled with some metallurgical calculation. Thus the simulation fully accounts for the different transformation kinetics during heating and cooling, which means that the "overall" specific heat in the calculation does take different values during heating and cooling,

as desired, even though the data used are deduced from a single experiment performed during heating.

Thermal diffusivity has also been measured, using the flash method at low temperatures and the "periodic" method[12] at higher ones. The results of this measurement are displayed in the right part of Fig. 2. Thermal conductivity is then obtained as the product of specific heat and thermal diffusivity.

These values are also used for the determination of the heat flux density absorbed by the upper face of the disk through an inverse method. The distribution of this density is given in Fig. 3. Also, the following values have been found for the convective and radiative heat transfer coefficients : H_c = 15 W/(m²°C), $H_r(T) = \varepsilon\sigma\left(T^2 + T_\infty^2\right).\left(T + T_\infty\right)$ with σ (Stefan's constant) = 5.67 10^{-8} W/(m²°K^4) and ε (thermal emissivity) = 0.75.

3.1.3 Metallurgy

For diffusional transformations, the phenomenological kinetic model proposed by Leblond and Devaux[14] is used. This model involves simple first-order evolution equations for the volume fractions of the phases, the parameters of which are determined using free dilatometry tests performed with austenitization conditions close to those encountered in the disk experiment[15]. The temperatures corresponding to the beginning and end of the austenitic transformation are 705 and 805°C respectively, and that corresponding to the beginning of the bainitic transformation, 565°C. The same model is used to reproduce tempering effects occurring near the HAZ, which are represented through some fictitious transformation from some as-quenched structure to some completely tempered one.

As for the martensitic transformation, the volume fraction z of martensite is assumed to be given as a function of temperature by Koistinen-Marburger's[16] famous formula :

$z(T)=1-\exp\left[-k(M_s-T)\right]$ (for $T \leq M_s$) with, for the material considered, $k = 2.47\ 10^{-2}°C^{-1}$ and M_s (starting temperature for the martensitic transformation) = 365°C.

3.1.4 Mechanics

As already mentioned, two calculations are performed, using the elastic-plastic and elastic-viscoplastic models. When viscous effects are accounted for, they are introduced at all temperatures, including those corresponding to metallurgical transformations. Transformation plasticity during the ferritic, bainitic and martensitic transformations is duly accounted for using the classical model of Leblond and coworkers[17,18], based on the seminal work of Greenwood and Johnson[19] and considering only the mechanism proposed by these authors to explain transformation plasticity. (The other mechanism[20] known to also be partly responsible for this phenomenon, during the martensitic transformation of certain steels, was experimentally shown by Desalos[21] to be negligible in the specific material considered here, and this was later confirmed by Cavallo[15], Coret[22] and Taleb and Grostabussiat[23]). Viscous effects are introduced in this model in an elementary, approximate way by simply allowing the yield stress of austenite to depend on strain rate in this phase (Vincent[24,25]). Both calculations without and with viscous effects make the assumption that hardening is of isotropic type and completely erased by all transformations (that is, the initial hardening of the newly formed phase is assumed to be zero). All calculations are performed with a large displacement, large strain option based on an updated Lagrangian formulation.

Since the main point in this paper is to show that viscoplastic calculations yield better results than plastic ones, as compared to experiments, it is essential to give details about the mechanical data used in both viscoplastic and plastic simulations. In the plastic calculation, the yield stresses and hardening curves of individual phases used are taken from the

experimental work of Dupas and Waeckel[26]. These authors measured these parameters as functions of temperature, for some relatively low strain rate roughly corresponding to that during the cooling period of the disk experiment. Thus, during the cooling stage of the calculation, the difference between the stress-strain curves used, taken from Dupas and Waeckel[26], and the "real" ones is small, of the order of 10 MPa. However, in the disk experiment, as in all welding processes, the strain rate is considerably higher during heating than during cooling, and therefore the yield stresses are also higher. Thus, during the heating stage of the calculation, the difference between the stress-strain curves used, corresponding to some low strain rate, and the "real" ones which ought to be used is larger, of the order of 50 MPa.

Of course, it would have been possible to use, in the plastic calculation, yield stresses and hardening curves corresponding to measurements performed at higher strain rates. But then these parameters would have been incorrect during cooling instead of heating. The point here is that owing to the important difference between values of the strain rate during heating and cooling, it is impossible, in purely plastic calculations disregarding the influence of strain rate, to use stress-strain curves "well fit" for both the heating and cooling periods. This is possible only in viscoplastic calculations accounting for this influence, and this is thought to be the basic reason why such calculations yield better results, as will be seen below.

With regard to the viscoplastic calculation, the mechanical parameters required have been determined from uniaxial creep tests. performed at INSA Lyon with a dilatometric device allowing for simultaneous thermal and mechanical measurements (Vincent[24,25]). These parameters have been measured between 400 and 700°C for bainite and martensite and between 700 and 1100°C for austenite. For example, the left part of Fig. 4 gives a comparison between experimental and computed creep curves at 1000°C. For lower and higher

temperatures, extrapolations are used. The validity of these measurements and extrapolations has been assessed by performing independent simple tension tests at different strain rates, and comparing predicted and experimental stress-strain curves. The difference between these curves is small, of the order of 10 MPa, for all strain rates envisaged. For example, the right part of Fig. 4 gives experimental and computed stress-strain curves at 1000°C.

Support conditions of the disk are schematized by prescribing a zero axial displacement at the node located on the lower face at a distance of 72 mm from its center.

All calculations are performed with the SYSWELD®[27] finite element program.

3.2 Results and discussion

3.2.1 Thermal and metallurgical analysis

The determination, by an inverse method, of the heat input distribution and the convective and radiative heat transfer coefficients leads to some very accurate thermal simulation, as can be seen in Fig 5 which compares experimental and computed thermal histories at 3 points on the upper and lower faces located at r = 0, 30 and 60 mm.

Fig. 6 compares the experimental and computed temporal evolutions of the temperature rate at the center of the lower face. These curves give informations about the occurrence of transformations through their effect (arising from latent heats) upon the evolution of temperature; it can thus be seen that at the point considered, the temperature rate is perturbed during heating between 35 and 55 s because of the austenitic transformation, and during cooling between 100 and 200 s, now because of the bainitic and martensitic transformations. Fig. 7 shows the computed HAZ on top, then the dimensions of the experimental HAZ below, and finally the measured and computed final proportions of bainite and martensite. (The

respective proportions of bainite and martensite in the HAZ cannot be read from the top part of the figure, they are provided only in its bottom part). The agreement between the dimensions of the experimental and computed HAZ is excellent. The measured and computed final proportions of bainite and martensite also compare very well.

3.2.2 Mechanical analysis

Evolution of the deformed structure:

Fig. 8 displays the temporal evolution of the axial displacement at a point located at r=1 mm on the lower face of the disk, and the final radial distribution of this displacement on both faces. There are some differences between experimental and computed results here, especially for the elastic-plastic simulation. First, prior to the austenitic transformation during heating, the collapse of the central part occurs somewhat too early in the plastic simulation. Moreover, at the end of heating, the axial displacement is overestimated by a factor of 2 in this simulation. The same overestimation can quite logically be observed in the final computed distribution of this displacement.

Detailed study of the temporal evolution of the axial displacement allows to better understand why such a discrepancy exists in the plastic simulation, and why it is greatly reduced in the viscoplastic one.

– $0 < t <$ 21-26 s : Raise of the central part of the disk

At the beginning of heating, temperature gradients appear in the radial and axial directions. The higher temperature on the upper face generates a bending effect which tends to raise the central part of the disk.

– 21-26 s $< t <$ 36 s : Collapse of the central part of the disk

At time t = 21 s in the plastic calculation, and 26 s in the viscoplastic one and the experiment, there is a sudden drop of the axial displacement. This effect comes from plastification of the central part of the disk, which occurs earlier on the hotter upper face than on the cooler lower one. Indeed, plasticity now limits compressive stresses on the upper face whereas they still increase on the lower one, and this generates a reversal of the bending moment and therefore a change of sign of the axial displacement.

The reason why the plastic calculation strongly overestimates this bending moment reversal, and consequently the drop of the axial displacement, is that it underestimates the yield stress and therefore the compressive stresses on the upper face. Of course, this is because, as explained above, the yield stresses used in this calculation are taken from experiments performed at strain rates corresponding to the cooling period, which are considerably lower than those encountered during the heating period discussed here. Accounting for viscous effects leads to enhancing the yield stress, decreasing the magnitude of the bending moment reversal and therefore also that of the drop of the axial displacement, in better agreement with the experiment.

- 36 s < t < 67 s : Austenitic transformation and end of the laser heating

At time t = 36 s, the austenitic transformation begins at the center of the upper face of the disk. This transformation induces a contraction of the central part of the upper face, which enhances the collapse of this central part. The austenitic transformation then propagates through the thickness down to the lower face. When the central part of the lower face starts transforming, the accompanying contraction tends to reverse the bending effect, which causes the central part of the disk to rise back till the end of the heating.

– t > 67 s : Cooling

During cooling, thermal contraction of the central part of the disk still induces a raise of this zone. After time t = 100 s, however, the axial temperature gradient becomes very small, so that the bending moments and the axial displacement do not change any longer, in spite of the large (but homogeneous through the thickness) expansion of the HAZ induced by the bainitic and martensitic transformations.

Residual strains:

Fig. 9 shows the distributions of radial and tangential residual strains, as measured using the numerical image correlation method. The zone investigated is a rectangle of dimensions 24.5×28.5 mm on the upper face of the disk. Also, Fig. 10 compares the measured and computed distributions of residual strains along some radial line on the upper face. The agreement is qualitatively acceptable for both simulations, but the plastic calculation slightly overestimates the maximum values of both the radial and tangential strains, which occur at the center of the disk. This is in line with the overestimation of the axial displacement in this simulation.

Residual stresses:

Fig. 11 and 12 provide the distributions of residual stresses on the lower and upper faces respectively. Both computed and experimentally determined values are reported, and also the mean width of the X-ray diffraction peak (noted L.I. in the figures).

Let us first discuss values of the width of the X-ray diffraction peak. This width is an increasing function of hardening and crystal lattice distortion; it increases in the following order : ferrite, bainite, martensite. Examination of its distribution thus allows for approximate determination of the zones where various transformations have occurred. Thus, in the central

HAZ which has undergone both bainitic and martensitic transformations, the peak width is larger than in the surrounding base material. Just outside the HAZ, it abruptly falls down to a minimum value (at r = 21 mm on the lower face and 24 mm on the upper face), then slightly increases again. This is typical of a zone which has undergone a tempering effect.

Let us now consider measured residual stresses. Correlating their values with the metallurgical structure, as determined from the width of the X-ray diffraction peak, one notes that the largest residual stresses are to be found on the periphery of the HAZ, in the partially austenitized zone and the tempered one. In contrast, residual stresses are relatively low (<150 MPa) in the HAZ. This is because the expansion induced by the bainitic and martensitic transformations, coupled with the additional plastic flow arising from transformation plasticity, partly compensates thermal contraction during cooling.

Let us finally compare experimental and computed values of the residual stresses. The agreement can be seen to be satisfactory for both the plastic and viscoplastic simulations, especially considering that experimental errors are at least of the order of 50 MPa; the magnitude and location of maximum values, in particular, are correctly predicted by both calculations. However, computed results are better on the upper face than on the lower one; indeed the calculation yields slightly compressive stresses in the HAZ on the latter face whereas tensile stresses are actually measured. Also, results of the viscoplastic simulation are slightly better, on average, than those of the plastic simulation.

It can be concluded that the influence of viscous effects upon residual stresses is marginal, in contrast to their influence on residual distortions.

4. Conclusion

An experimental mockup of a welded structure developed at INSA Lyon and especially designed for the analysis of the material behavior in the heat affected zone has been described. Numerical simulations of this mockup using both elastic-plastic and elastic-viscoplastic models have been performed and compared to experiments. The comparison has clearly shown that viscous effects have a marginal influence upon residual stresses but an important one upon residual distortions, and must be accounted for if accurate predictions of the latter quantities are desired; in the case investigated, the value of the residual axial displacement predicted by the plastic simulation is erroneous by as much as a factor of 2.

This conclusion is in line with that of the works of Bru *et al*[28] and Leblond *et al.*[29], who found that values of the yield stress at very high temperatures, close to the fusion point, which could be expected to be of minor importance in numerical simulations of welding, in fact have a significant influence on predicted residual distortions. (Such temperatures were not reached in the experiments described here since fusion was deliberately avoided, as explained above). It thus appears that *residual distortions are sensitive to tiny details of the material law which have little influence on residual stresses*. This makes accurate prediction of residual distortions a considerably more difficult challenge than that of residual stresses, especially in large thin welded structures (as encountered for instance in the automotive industry) for which these distortions can be quite large.

One final remark is that the general need for accurate description of the material behavior at high temperatures (including, in particular, viscous effects), becomes even clearer in investigations of effects occurring near the weld at such temperatures, like hot cracking for instance.

References

1. Bergheau J.-M., Leblond J.-B., 1991, "Coupling between heat flow, metallurgy and stress-strain computations in steels - The approach developed in the computer code SYSWELD for welding or quenching", in "Modeling of Casting, Welding and Advanced Solidification Processes V", Rappaz, Ozgu and Mahin, eds., the Minerals, Metals and Materials Society, pp. 203-210.

2. Dong Y., Hong J.K., Tsai C.L., Dong P., 1997, "Finite element modeling of residual stresses in austenitic stainless steel pipe girth welds", Welding J., 76, 442-449.

3. Giusti J., 1981, "Contraintes et déformations résiduelles d'origine thermique – Application au soudage et à la trempe des aciers", Ph.D. thesis, Université Paris VI.

4. Gu M., Goldak J., 1991, "Mixing thermal shell and brick elements in FEA of welds", Proceedings of the 10th International Conference on "Offshore Mechanics and Arctic Engineering", Stavanger, Norway, publication of the ASME, vol. III, part A, pp. 1-6.

5. Josefson B.L., 1991, "Prediction of residual stresses and distortions in welded structures", Proceedings of the 10th International Conference on "Offshore Mechanics and Arctic Engineering", Stavanger, Norway, publication of the ASME, vol. III, part A, pp. 25-30.

6. Lindgren L.E., 2001, "Finite element modeling and simulation of welding, Part 1 – Increased complexity; Part 2 – Improved material modelling; Part 3 – Efficiency and integration", J. Thermal Stresses, 24, 141-192; 195-231; 305-334.

7. Lindgren L.E., 2002, "Welding simulation – Knowing what is not necessary to know", Math. Modelling of Weld Phenomena, 6, 491-518.

8. Näsström M., Wikander L., Karlsson L., Lindgren L.E., 1992, “Combined 3D and shell modelling of welding”, Proceedings of the IUTAM Symposium on “Mechanical Effects of Welding”, Lulea, Sweden, Springer-Verlag, pp. 197-206.

9. Oddy A., Lindgren L.E., 1997, “Mechanical modelling and residual stresses”, in “Modeling in Welding, Hot Powder Forming and Casting”, L. Karlsson, ed., ASM International, pp. 31-59.

10. Ueda Y., Nakacho K., Yuan M., 1991, “Theoretical analysis : measurement and prediction of welding residual stresses using FEM”, Proceedings of the 10th International Conference on “Offshore Mechanics and Arctic Engineering”, Stavanger, Norway, publication of the ASME, vol. III, part A, pp. 7-15.

11. Wang Z.G., Inoue T., 1985, “Viscoplastic constitutive relation incorporating phase transformation - Application to welding”, Materials Sci. Technol., 1, 899-903.

12. Mguil-Touchal S., Morestin F., Brunet M., 1996, “Mesure de champs de déplacements et de déformations par corrélation d'images numériques”, Proceedings of “Colloque National Mécamat 96 - Mécanisme et Mécanique des Grandes Déformations”, pp. 179-182.

13. Blanc G., Druette L., Laurent M. and Raynaud M., 1998, “Etudes des propriétés thermiques de l’acier 16MND5”, Centre de Thermique INSA Lyon Internal Report n° 20113809E.

14. Leblond J.B., Devaux J., 1984, “A new kinetic model for anisothermal metallurgical transformations in steels including effect of austenite grain size”, Acta Met., 32, 137-146.

15. Cavallo N., 1998, “Contribution à la validation expérimentale de modèles décrivant la ZAT lors d'une opération de soudage”, Ph.D. thesis, INSA Lyon.

16. Koistinen D.P., Marburger R.E., 1959, “A general equation prescribing extent of austenite-martensite transformation in pure Fe-C alloys and plain carbon steels”, Acta Met., 7, 59-60.

17. Leblond J.B., 1989, “ Mathematical modelling of transformation plasticity in steels – II. Coupling with strain hardening phenomena ”, Int. J. Plasticity, 5, 573-591.

18. Leblond J.B., Devaux J., Devaux J.C., 1989, “Mathematical modelling of transformation plasticity in steels – I. Case of ideal-plastic phases”, Int. J. Plasticity, 5, 551-572.

19. Greenwood G.W., Johnson R.H, 1965, “The deformation of metals under small stresses during phase transformation”, Proc. Roy. Soc., 283, 403-422.

20. Magee C.L, 1966, “Transformation kinetics, microplasticity and ageing of martensite in Fe-3lNi”, Ph.D. thesis, Carnegie Mellon University, Pittsburg.

21. Desalos Y., 1981, “Comportement dilatométrique et mécanique de l’austénite métastable d’un acier A533”, IRSID Report n° 95349401 MET 44.

22. Coret M., 2001, “Etude expérimentale et simulation de la plasticité de transformation et du comportement multiphase de l’acier de cuve 16MND5 sous chargement multiaxial anisotherme”, Ph.D. thesis, LMT Cachan.

23. Taleb L., Grostabussiat, S., 1998, “Etude du comportement mécanique des aciers en cours de transformations métallurgiques – Analyse de la déformation irréversible dans les essais de plasticité de transformation”, INSA Lyon/URGC-Structures Internal Report n° 1/972/005c.

24. Vincent Y., 2002, “Simulation numérique des conséquences métallurgiques et mécaniques induites par une opération de soudage - Acier 16MND5”, Ph.D. thesis, INSA Lyon.

25. Vincent Y., Bergheau J.M., Leblond J.B., Jullien J.F., 2003, “Viscoplastic behaviour of steels during phase transformations”, submitted to Comptes-Rendus Mécanique.

26. Dupas P., Waeckel F., 1994, “Recueil bibliographique de caractéristiques thermo-mécaniques pour l’acier de cuve, les revêtements inoxydables et les alliages 182 et 600”, EDF/DER Internal Report HI-74/93/097, HT-26/93/058A.

27. SYSWELD, 2002, User’s Manual, Engineering Systems International.

28. Bru D., Devaux J., Bergheau J.-M. and Pont D., 1996, “Influence of material properties at high temperatures on the modelling of welding residual stress and deformation state”, Mathematical Modelling of Weld Phenomena 3, edited by Pr. H. Cerjak, The Institute of Materials, London, pp. 456-463.

29. Leblond J.B., Pont D., Devaux J., Bru D., Bergheau J.M., 1997, “Metallurgical and mechanical consequences of phase transformations in numerical simulations of welding processes”, in “Modeling in Welding, Hot Powder Forming and Casting”, L. Karlsson, ed., ASM International, pp. 61-89.

Figure captions

Figure 1 : Sketch of the experimental device

Figure 2 : Measured thermal properties

Figure 3 : Heat flux distribution

Figure 4 : Thermal histories at 3 points of the upper and lower faces (r =0, 30, 60 mm)

Figure 5 : Temperature rate as a function of time at the center of the lower face

Figure 6 : Dimensions of HAZ on the lower and upper faces and final phase proportions

Figure 7 : Vertical displacement vs. time on the lower face at r=1 mm, and vs. radial distance on both faces at the end of the process

Figure 8 : Distributions of measured residual radial (left) and tangential (right) strains

Figure 9 : Residual radial and tangential strains as functions of radial distance on the upper face

Figure 10 : Residual radial and tangential stresses on the lower face

Figure 11 : Residual radial and tangential stresses on the upper face

Figures

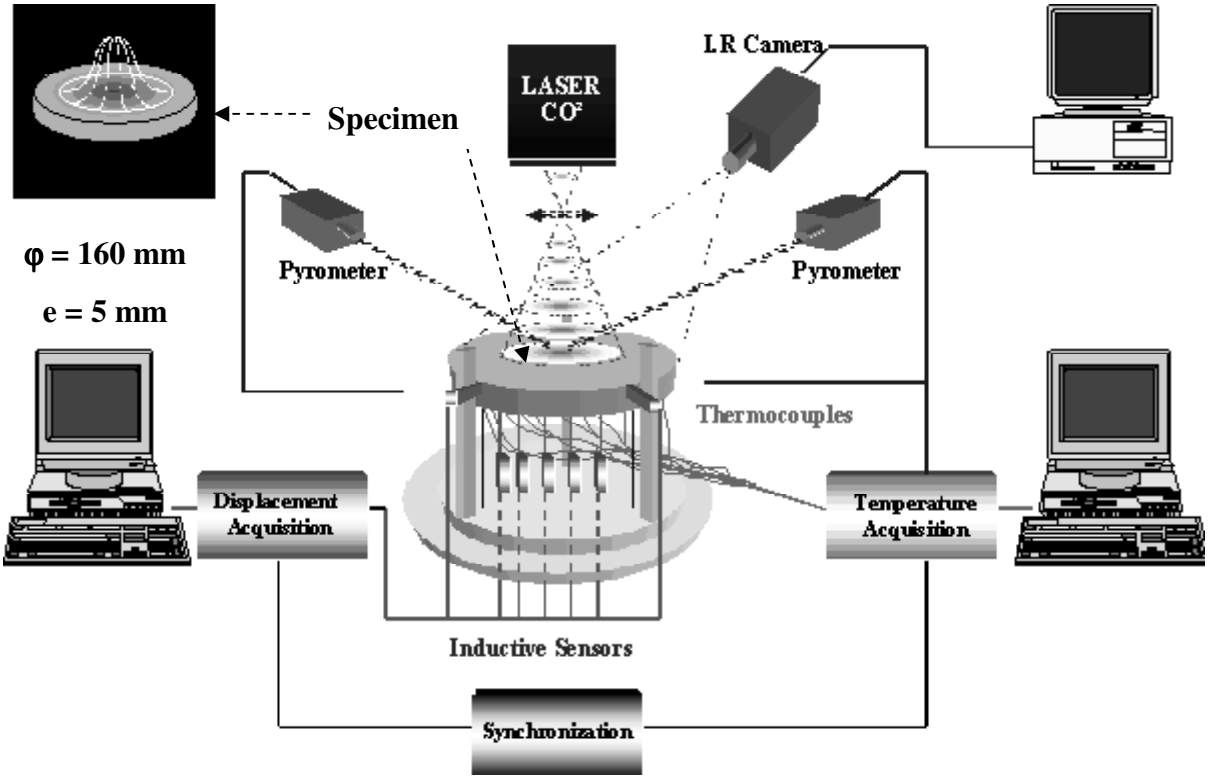

Figure 1 : Sketch of the experimental device

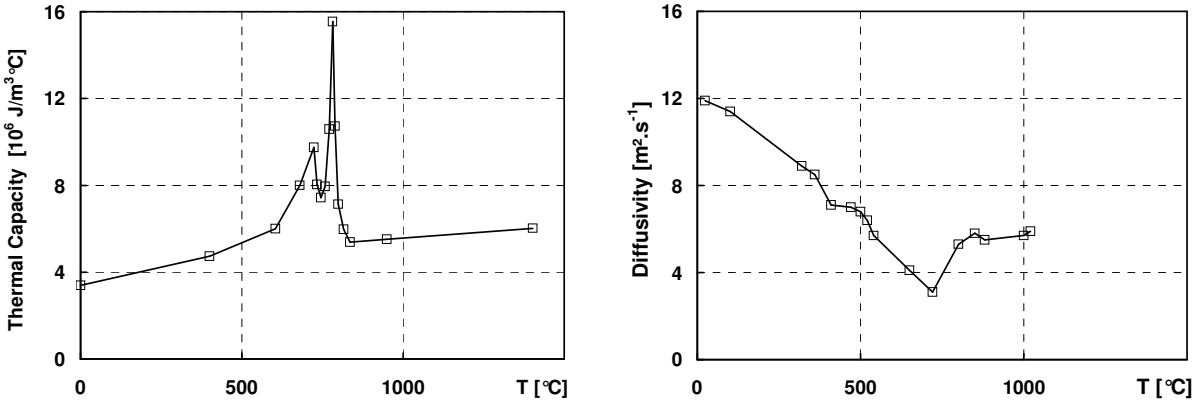

Figure 2 : Measured thermal properties

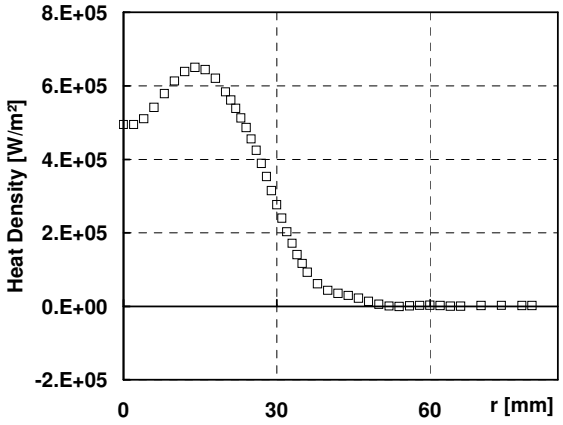

Figure 3 : Heat flux distribution

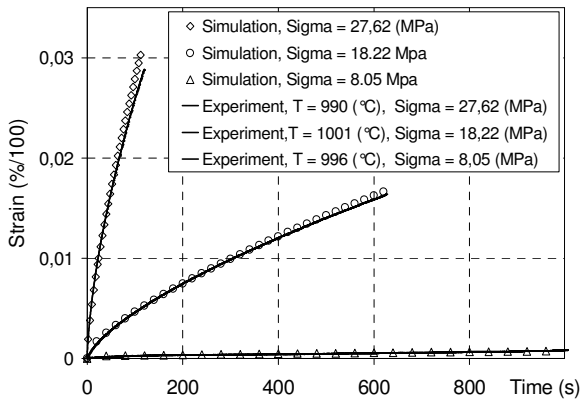

Creep curves, Temperature 1000°C, Austenite

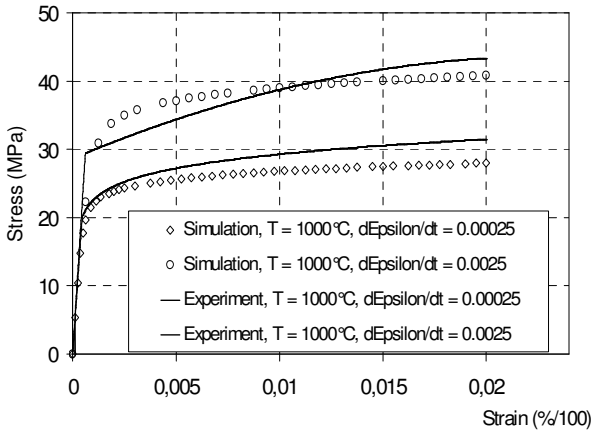

Tensile Curves, Temperature 1000°C, Austenite

Figure 4: Experimental and computed creep and tensile tests.

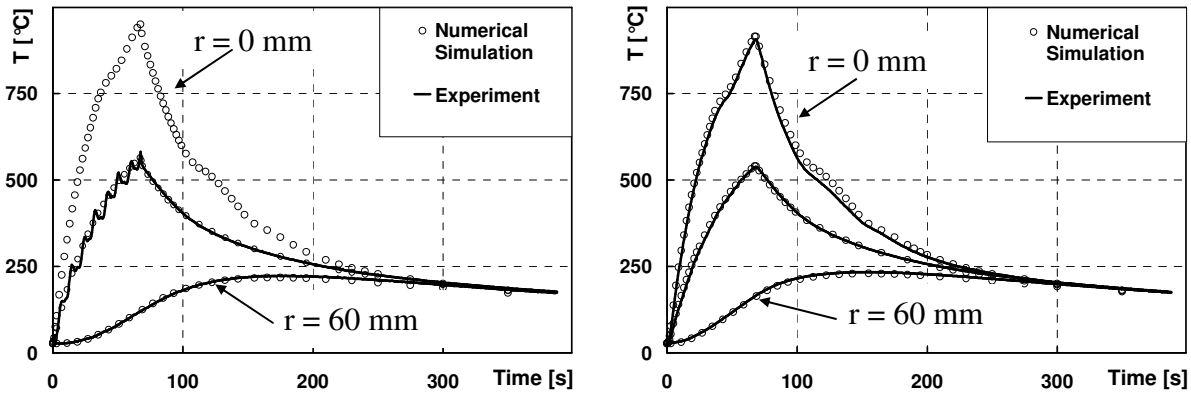

Figure 5 : Thermal histories at 3 points of the upper and lower faces (r=0, 30, 60 mm)

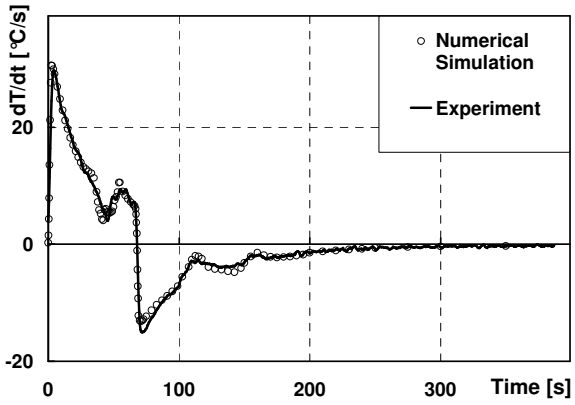

Figure 6 : Temperature rate as a function of time at the center of the lower face

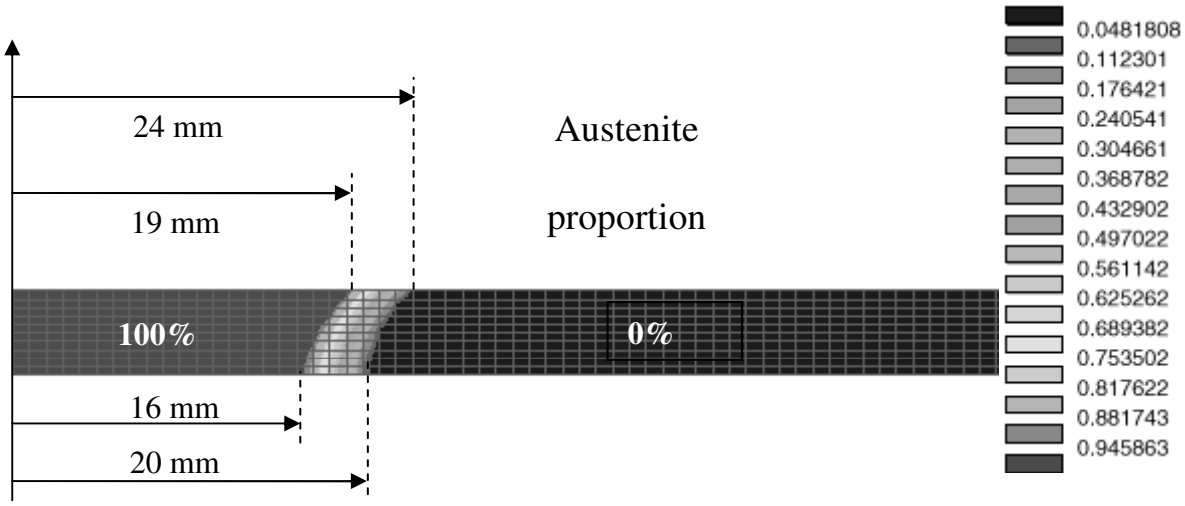

Experiment	Totally austenitized zone	Partially austenitized zone
Upper face	19 mm	4 mm
Lower face	16 mm	4 mm

	Experiment	Simulation
Martensite proportion	[27 – 38] %	32.5 %
Bainite proportion	[62 – 73] %	67.5 %

Figure 7 : Dimensions of HAZ on the lower and upper faces and final phase proportions

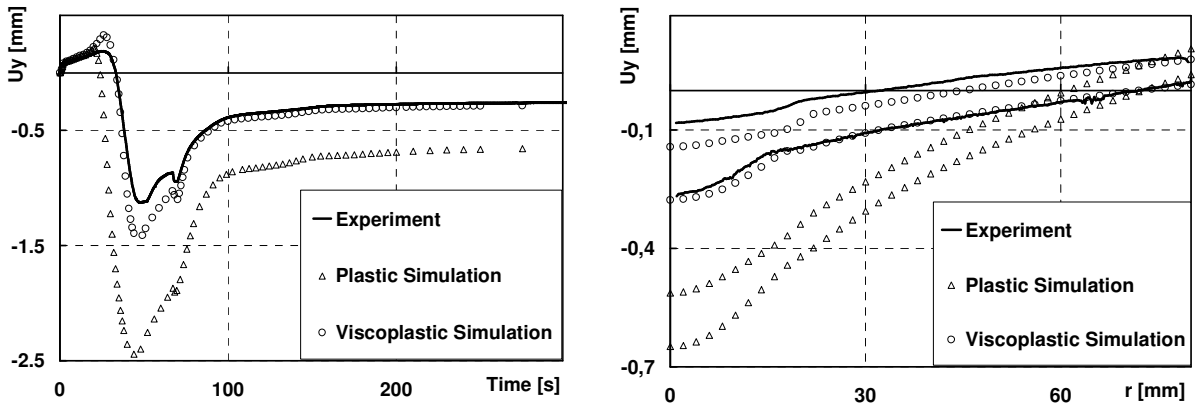

Figure 8 : Vertical displacement vs. time on the lower face at r=1 mm, and vs. radial distance on both faces at the end of the process

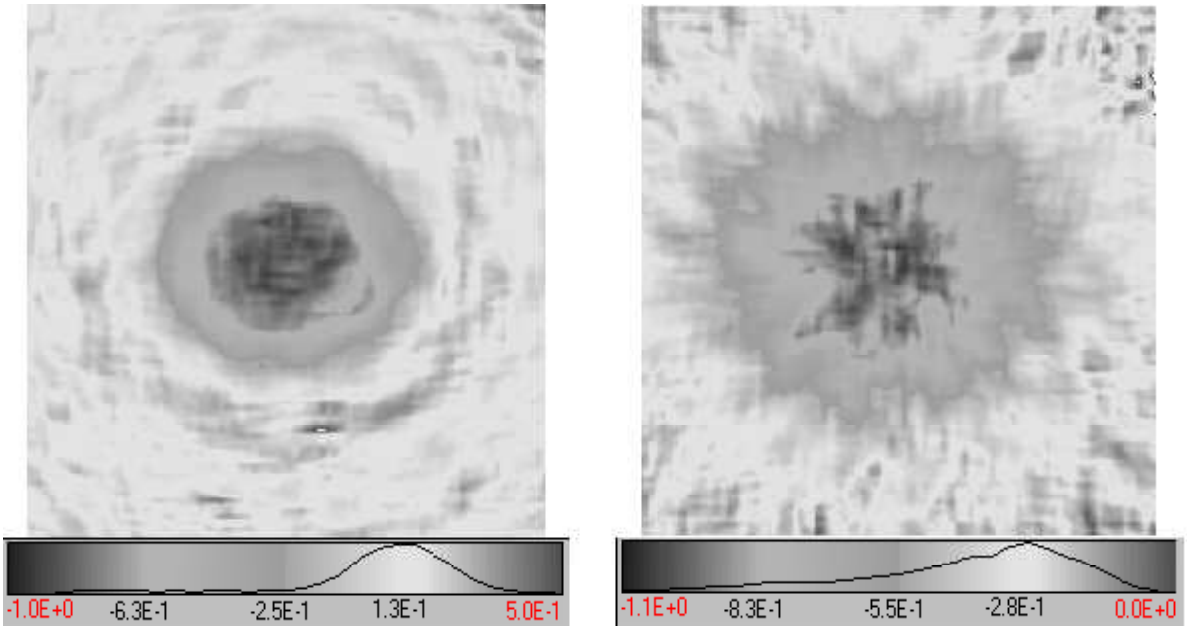

Figure 9 : Distributions of measured residual radial (left) and tangential (right) strains

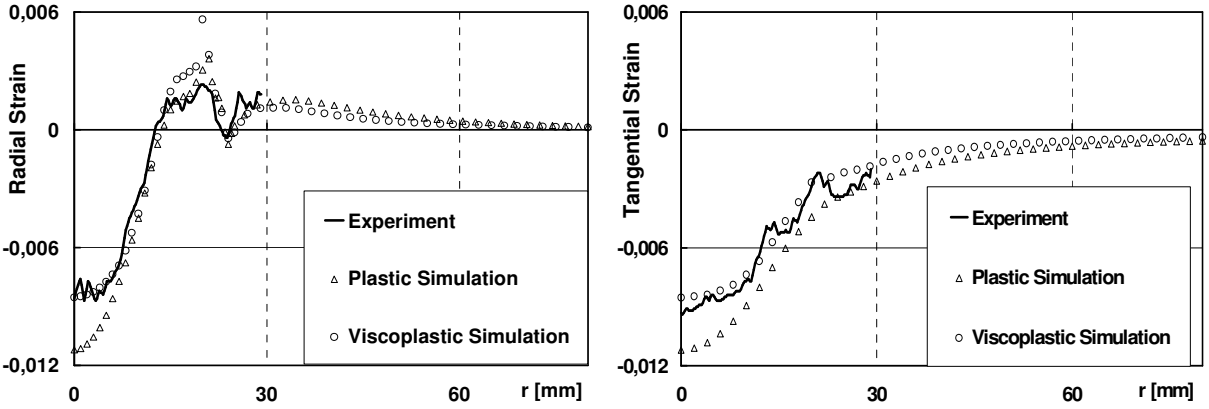

Figure 10 : Residual radial and tangential strains as functions of radial distance on the upper face

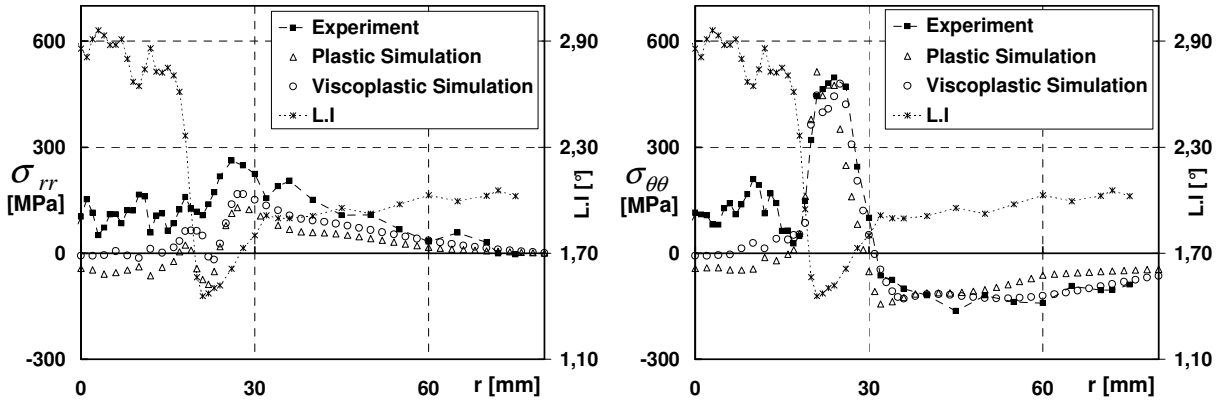

Figure 11 : Residual radial and tangential stresses on the lower face

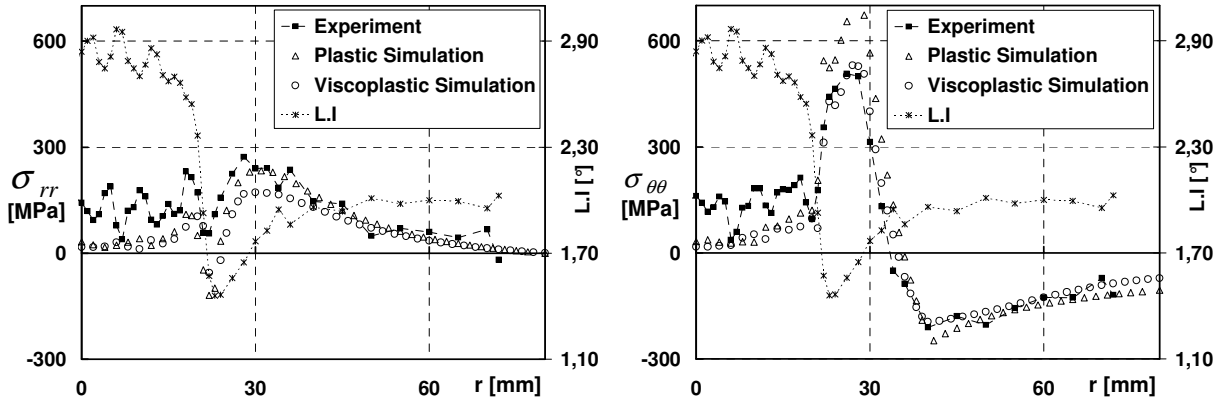

Figure 12 : Residual radial and tangential stresses on the upper face

Table captions

Table 1 : Chemical composition of 16MND5 steel (French standard)

Tables

	C	Si	Mn	Ni	Cr	Mo	Al	Sn	S	P	N
Min	0.196	0.22	1.51	0.63	0.19	0.51	0.021	< 20 ppm	< 0.002	< 0.002	< 0.004
Max	0.212	0.23	1.58	0.65	0.20	0.53	0.024				

Table 1 : Chemical composition of 16MND5 steel (French standard)